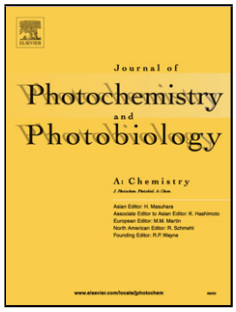

Title: Promotional effect of Rh nanoparticles on WO_3/TiO_2 titanate nanotube photocatalysts for boosted hydrogen production

Authors: R. Camposeco, S. Castillo, V. Rodriguez-González, M. Hinojosa-Reyes, María I. Medina-Álvares, Isidro Mejía-Centeno

PII: S1010-6030(17)30670-6
DOI: https://doi.org/10.1016/j.jphotochem.2017.11.014
Reference: JPC 10998

To appear in: *Journal of Photochemistry and Photobiology A: Chemistry*

Received date: 17-5-2017
Revised date: 22-8-2017
Accepted date: 9-11-2017

Please cite this article as: R.Camposeco, S.Castillo, V.Rodriguez-González, M.Hinojosa-Reyes, María I.Medina-Álvares, Isidro Mejía-Centeno, Promotional effect of Rh nanoparticles on WO3/TiO2 titanate nanotube photocatalysts for boosted hydrogen production, Journal of Photochemistry and Photobiology A: Chemistry https://doi.org/10.1016/j.jphotochem.2017.11.014

Promotional effect of Rh nanoparticles on WO_3/TiO_2 titanate nanotube photocatalysts for boosted hydrogen production

R. Camposeco[a*], S. Castillo[b], V. Rodriguez-González[a], M. Hinojosa-Reyes[c], María I. Medina-Álvares[d], Isidro Mejía-Centeno[e]

[a]*Instituto Potosino de Investigación Científica y Tecnológica, División de Materiales Avanzados, 78216-San Luis Potosí, S.L.P.; México*
[b]*Dirección de Tecnología del Producto, Instituto Mexicano del Petróleo, 07730-México City; México*
[c]*Facultad de Ciencias, Universidad Autónoma de San Luis Potosí, San Luis Potosí, 78000-San Luis Potosí, S.L.P.; México.*
[d]*Centro Interdisciplinario de Investigaciones y Estudios sobre Medio Ambiente y Desarrollo, Instituto Politécnico Nacional, 07340-Mexico City; México.*
[e]*Dirección de Investigación en Transformación de Hidrocarburos, Instituto Mexicano del Petróleo, 07730-México City; México*

*Corresponding author.
Tel: + (55) 52- 9175-8216;
Fax: + (55) 52- 9175-9699
E-mail address: roberto.camposeco@ipicyt.edu.mx

Graphical Abstract

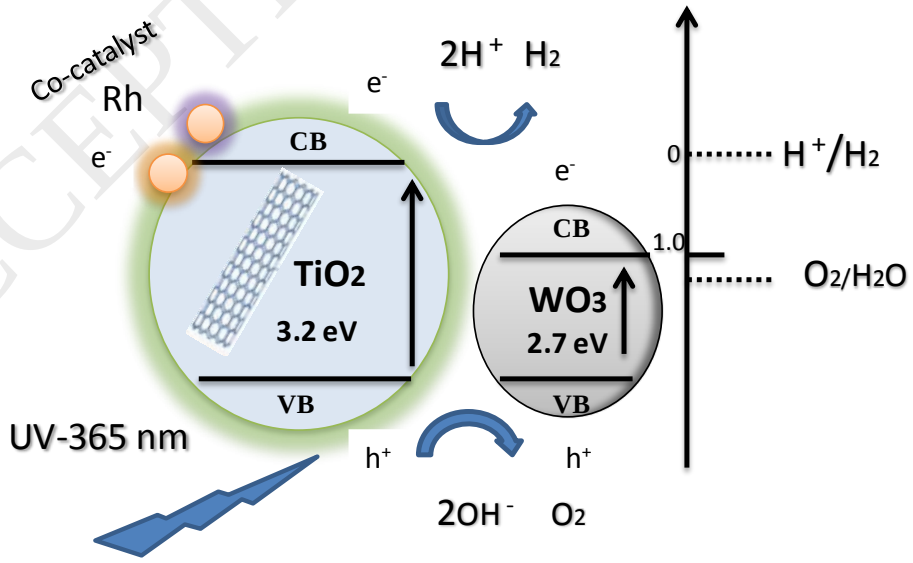

Highlights

- Titanate nanotubes were synthesized by microwave irradiation.
- Rhodium nanoparticles were loaded on WO_3/NT photocatalysts.
- Rh-WO_3/NT shows remarkably photocatalytic activity under UV light and visible light
- Rh acts as co-catalyst of WO_3/NT, while WO_3 stabilizes the structure of nanotubes
- The diagram of density of states (VB and CB) can be determined from UV-vis and XPS

Abstract

In this work, we explore the hydrogen production via the water splitting process on Rh-WO_3 photocatalysts supported on nanotubes of TiO_2. H_2 production tests were performed in a 2-propanol-water solution. The support (titanate nanotubes, NT) was obtained, first, by the sol-gel method followed by, second, the hydrothermal method. The surface of the titanate nanotubes was decorated with nanoparticles of rhodium and tungsten by applying microwave irradiation. The photocatalysts were characterized by XRD, HR-TEM, UV-vis, S_{BET}, H_2-TPR and XPS.

For the photocatalytic tests, we employed two photocatalysts with 0.3 and 0.5 wt. % of Rh on WO_3/TiO_2 (3 wt.% of WO_3) under UV-A light radiation at 365 nm and visible light at 450 nm. We found that 56 μmol h^{-1} of hydrogen were produced by photolysis. The support (NT) produced 59 μmol h^{-1} of hydrogen. The addition of 3 wt.% of WO_3 to the nanotubes increased slightly the H_2 production (66 μmol h^{-1}). However, a promotional effect was observed when rhodium was added to the 3WO_3/NT photocatalysts. In fact, the highest hydrogen production was obtained on the 0.5Rh-3WO_3/NT photocatalyst (234 μmol h^{-1}), even after seven cycles of 8 h. We suggest that Rh acts as co-catalyst of the WO_3 during the water splitting process. A diagram for the density of states, based on the UV-vis and XPS results, is proposed.

Keywords: Titanate nanotubes; Rh co-catalyst: visible response; H_2 production.

1. Introduction

Titanium dioxide and tungsten trioxide possess properties such as electronic band structure, high photoactivity, chemical stability, and low cost that make them good candidates for photocatalytic reactions [1-2]. Titanium dioxide has shown relatively large band gap energies (3.0–3.2 eV) and the ability to absorb only ultraviolet (UV) light. In order to develop photocatalysts with improved photocatalytic activity, the reduction of the semiconductor band gap in TiO_2 is a possible way to

reach this goal. In this sense, WO_3 is an important metal-oxide semiconductor that presents relatively low band gap energies (2.6-2.8 eV) [3-4]. Likewise, there are studies [5-6] that have been focused on the coupling mechanism between WO_3 and TiO_2. Nevertheless, most of these studies have reported on WO_3/TiO_2 photocatalysts in the form of traditional particle shapes such as spheres and thin films [5-6]. In fact, there are few studies focused on the growth of 1D-highly-ordered-WO_3–TiO_2-titanate nanotubes. Recently, WO_3/TiO_2 nanotube systems and various methods of synthesis, such as sol–gel, hydrothermal and anodization, which have been employed to incorporate WO_3 into TiO_2 nanotubes, have attracted considerable attention [7-9].

Hydrogen production by water splitting is highly effective by using nanoparticles of noble metals such as Pt or Au on TiO_2 supports [10]. Other noble metals that have been employed in the H_2 production due to their low cost are Ag, Cu, and Ni, but they have shown themselves to be less effective [11-12]. Highly dispersed metal nanoparticles can improve the photocatalytic performance of the photocatalyst, leading to a lower charge carrier recombination rate in the semiconductor during the water splitting reaction, which is an effective way to restrain the recombination of photo-generated-electron–hole pairs [13]. However, the morphology control of WO_3 nanostructures in the form of nanorods, nanotubes and nanowires is difficult and WO_3 alone cannot produce H_2 from water owing to insufficient energy of its conduction band for H_2O reduction. An alternative to improve the hydrogen production from water is the loading of co-catalysts. NiOx, RuO_2, and Rh−Cr, for example, are effective co-catalysts for increasing the activity of various photocatalysts in water decomposition. In fact, it has been reported [14-16] that PdS, MoS_2 and NiS co-catalysts increase the photocatalytic activity.

In this work, we report the photocatalytic activity of Rh and WO_3 supported on titanate nanotubes (NT) for the hydrogen production via the water splitting process. The effect of 3 wt.% of WO_3 supported on NT is analyzed. We also surveyed the effect of 0.3 and 0.5 wt.% of rhodium supported

on $3WO_3$/NT upon hydrogen production by photoreaction. As reference, we also employed commercial TiO_2 (P25) as support. For the stability test, our best photocatalyst (0.5Rh-$3WO_3$/NT) was tested during seven cycles of eight hours each one. The main objective of this work was to establish the effectiveness of our photocatalysts for the hydrogen production by the water splitting process, as well as to investigate the effect rhodium nanoparticles as co-catalyst supported on $3WO_3$/NT upon hydrogen production.

2. Experimental

2.1 Preparation of Rh-WO_3/TiO_2 by sol-gel method

TiO_2-nanocrystals were prepared by the sol-gel method as follows: 36.6 ml of titanium (IV) isopropoxide (Aldrich 97%) were dissolved in 145 ml of 2-propanol (Baker 99.9%). The solution was set under constant stirring. HNO_3 was added to adjust the reaction medium at pH 2. Simultaneously, *in-situ* was added the appropriate amounts of tungstic acid (99%, Sigma-Aldrich) to obtain 3 wt.% of WO_3 and rhodium (III) chloride hydrate (99.98%, Sigma-Aldrich) to obtain materials with 0.3 and 0.5 wt.% of Rh. The hydrolysis was accomplished by adding bidistilled water. The solution was then maintained under stirring and reflux until the gel was formed. Afterwards, the gel was dried at 80ºC for 12 h, and annealed at 300°C for 4 h.

For comparative purposes, P25 (from Degussa) was used as support. In this case, the photocatalysts were prepared by the incipient impregnation method by using 0.5 wt.% of rhodium and 3 wt.% of WO_3 using the precursors mentioned above, both in aqueous solution. The impregnated P25 was dried at 80°C for 12 h and annealed at 300°C for 4 h.

2.2. Preparation of Rh-WO_3/NT by hydrothermal method

Titanate nanotubes (NT) were synthesized by the hydrothermal method. The hydrothermal synthesis was carried out using a NaOH solution (10 N) in a microwave oven at 150°C for 4 h at 400 rpm. The slurry was washed several times with a HCl solution until reaching pH 3; then, it was washed with distilled water until pH was close to 7, and finally, it was filtered and dried at 80°C for 12 h. The annealing process was carried out at 300°C for 4 h. It is important to note that the addition of WO_3 and Rh to obtain materials with 3 wt.% of WO_3, 0.3 and 0.5 wt.% of Rh was done during the sol-gel method. Tungstic acid (H_2WO_4) and rhodium (III) chloride hydrate were used as precursors. The catalysts were labeled as $3WO_3$/NT, 0.3Rh-$3WO_3$/NT and 0.5Rh-$3WO_3$/NT. The label NT corresponds to the titanate nanotubes structure, as support.

2.3. Photocatalytic water splitting

Photocatalytic water splitting to generate hydrogen was carried out in a quartz photo-reactor. A UV lamp (λ=365 nm or λ=450 nm) was used during the experiment. The quartz photo-reactor had a full operation volume of 250 ml. The scavenger solutions consisted of water-2-propanol (100:100 mL, 50 vol. % of H_2O). During the photocatalytic tests, samples of 50 mg of photocatalyst were used and stirred for 5 min while the system was purged with nitrogen to remove the dissolved oxygen from the solution.

Analyses were conducted on a gas chromatograph (Trace GC Ultra, Thermo Scientific) equipped with a thermal conductivity detector and with a 5-Å molecular sieve packed column. Nitrogen was used as the carrier gas at a flow rate of 30 cm^3 min^{-1}. The system was calibrated previously to quantify the hydrogen production. In order to analyze the hydrogen produced by the scavenger solution, the respective photolysis water-2-propanol was carried out. To corroborate the effect of the 2-propanol in the water splitting test, a photocatalysis experiment was also carried out only

with water.

For the stability test, seven cycles of 8 h each one were carried out for the selected most active photocatalyst (0.5Rh-3WO_3/NT) and three cycles for 0.5Rh/NT to corroborate the effect of tungsten upon photocatalytic stability. After running the experiments, the UV lamp was turned off, the produced hydrogen was released and the reaction system was purged with nitrogen until the hydrogen chromatographic signal was zero. Afterwards, the reactor system was sealed, after 8 h, the lamp was turned on again to start the next cycle and so on until the third cycle was completed.

2.4. Characterization

X-ray diffraction (XRD) patterns of the samples packed in a glass holder were recorded at room temperature with Cu Kα radiation in a Bruker Advance D-8 diffractometer. The data were collected for scattering angles (2θ) ranging from 4 to 80° with a step size of 0.02° for 2 s per point. Microscopy (HR-TEM) analyses of the samples were performed in a JEOL 2010F microscope operating at 200 kV and equipped with a Schottky-type field emission gun and an ultrahigh resolution pole piece (Cs = 0.5 mm, point-to-point resolution, 0.190 nm).

Textural properties were determined in an ASAP-2000 analyzer from Micrometrics. The specific surface area was calculated from the Brunauer–Emmet–Teller (BET) equation from N_2 physisorption at 77 K. A Nicolet, pro-evolution 600, UV–vis spectrometer was used to record directly the diffuse reflectance spectra (DRS).

The H_2-TPR study of the photocatalysts was performed in a Quantachrome ChemBET TPR/TPD chemisorption analyzer unit under a flow of 10% H_2/Ar gas mixture (20 ml min^{-1}) with a heating rate of 10°C min^{-1} from room temperature up to 600°C. XPS was performed with a Thermo VG Scientific Escalab 250 spectrometer equipped with a hemispherical electron analyzer and an Al Kα radiation source (1486.6 eV) powered at 20 kV and 30 mA, respectively. The binding energy was

determined by using carbon C (1s) as reference line (284.6 eV). The spectrometer was operated at pass energy of 23.5 eV, and the base pressure in the analysis chamber was maintained in the order of 3×10^{-8} mbar. Peak fitting was done by using XPSPEAK 41 with Shirley background.

3. Results and Discussions

3.1. XRD and BET

Fig. 1(a) presents the XRD patterns for the titanate nanotubes (NT) and the $3WO_3$/NT, 0.3Rh-$3WO_3$/NT and 0.5Rh-$3WO_3$/NT photocatalysts annealed at 300°C. The main phase observed is tritanic acid ($H_2Ti_3O_7$) according to JCPDS 36-0654 and the characteristic bands located at 2θ = 9.79° (100), 24.37° (110), 28.3° (311), and 48.5° (020). Moreover, the peaks located at 23.62° and 29.16°, corresponding to the (020) and (120) crystal planes of the monoclinic WO_3 phase, were not observed. Likewise, the peaks related to rhodium nanoparticles were not observed due to the fact that XRD analysis was not sensitive enough to detect very low rhodium contents. However, the addition of WO_3 to the nanotubes increases the intensity of peaks located at 2θ = 9.79°, 24.37° and 28.3°. The presence of 0.3 and 0.5 wt.% of Rh diminishes the intensity of the peaks located at 2θ = 24.37° and 28.3° notably respect to $3WO_3$/NT. The intensity of the peak located at 2θ = 9.79°, that is ascribed to the scrolling of the titanate nanotubes [17-18], remained constant.

XRD patterns for the spent 0.5Rh-$3WO_3$/NT photocatalyst annealed at 300°C was carried out to verify the structural stability and the changes suffered during photocatalyst tests. Fig 1(a) shows that the peak located at 2θ = 9.7° (100) was shifted to 12.40°. The corresponding **d** spacing for the 2θ = 9.7° is 9.11 nm, for 2θ = 12.40° is 7.17 nm. This effect could be due to the shift towards larger angles, which in turn was due to a decrease in the interlayer spacing in the titanate nanotube walls.

The decreases in the interlayer spacing was accompanied by the removal of H_2O in the structure of titanate nanotube [18]. Another effect observed in the spent 0.5Rh-3WO_3/NT photocatalyst is the presence of the anatase phase in the XRD pattern due to titanate nanotubes are deteriorated.

N_2 adsorption-desorption for the NT, 3WO_3/NT, 0.3Rh-3WO_3/NT and 0.5Rh-3WO_3/NT annealed at 300°C are shown in Fig. 1(b). These isotherms can be classified as type IV with an H3 hysteresis loop that is characteristic of parallel sheets [19]. The results of BET surface areas of the NT, 3WO_3/NT, 0.3Rh-3WO_3/NT and 0.5Rh-3WO_3/NT samples were 290, 292, 270 and 320 m^2 g^{-1}, respectively. Table 1 shows the specific area and the phase of the materials used in this work. As it can be seen, the surface area is not affected by the addition of rhodium and tungsten to the titanate nanotubes.

3.2. Morphology by HR-TEM

In order to confirm the morphology, size and shape of the Rh and WO_3 nanoparticles, the NT, 3WO_3/NT, and 0.5Rh-3WO_3/NT photocatalysts annealed at 300°C were analyzed by HR-TEM. Fig. 2(a) shows the micrograph for the titanate nanotubes (NT) as support. The image presents well-defined nanotubes with an inner diameter of 4 nm and external diameter close to 10 nm. The thickness of the nanotubular walls is around 2 nm with a thickness space of 0.75 nm.

Fig. 2(b) reveals that the WO_3 nanoparticles, with an average diameter of 1 nm, are uniformly distributed on both side of the walls of the titanate nanotubes. In fact, there are more WO_3 nanoparticles on the inside wall than on the outside wall of the titanate nanotubes for the 3WO_3/NT photocatalyst. With regard to the 0.5Rh-3WO_3/NT photocatalyst, reported on Fig. 2(c), we confirm the presence of rhodium nanoparticles with sizes between 1 and 2 nm in the channel of the tubular structure, reaching less dispersion with respect to tungsten nanoparticles. The presence of rhodium and tungsten nanoparticles in the titanate nanotube was confirmed by EDS (not showed).

Fig. 2(d) shows the HR-TEM for the spent 0.5Rh-3WO_3/NT photocatalyst after reaction. We found that a cluster, with the anatase phase, appears surrounding the nanotube. Besides, the length and width of the nanotubes is affected notably. It is possible to appreciate a mixture of short and long nanotubes due to deteriorate of initial structure of the titanate nanotubes. However, it is important to mention that the tubular structure remained after seven cycles of reaction.

3.3. UV-vis

Fig. 3 shows the UV-vis absorption spectra for NT, WO_3/NT and Rh-WO_3/NT photocatalysts in the 200-700 nm region. The NT support showed absorption at around 400 nm while the 3WO_3/NT photocatalyst showed absorbance in the wavelength region of 420 nm with a red shift adsorption. When WO_3 and TiO_2 form a coupled photocatalyst, the creation of defective energy levels within the band gap (Eg) decreases the band gap energy [20], as in the case of the 3WO_3/NT photocatalyst, while the addition of rhodium (0.3 and 0.5 wt. %) to the 3WO_3/NT photocatalyst displays a remarkable blue shift absorption at 380 and 350 nm, respectively, which can be due to the dispersion of rhodium nanoparticles on the 3WO_3/NT photocatalysts. On the other hand, when the particle size decreases below its size at minimum band gap, the traps shift to higher energy levels, resulting in blue shifting absorption spectra promoted by the size quantization effect [21]. Table 1 shows the calculated band gap for the photocatalysts used in this work.

3.4. H_2-TPR

Fig. 4 shows the H_2 TPR for the NT, WO_3/NT and Rh-WO_3/NT photocatalysts. The NT shows a peak reduction centered at 480°C. The addition of 3 wt.% of WO_3 to the titanate nanotubes modify the TPR profile of the nanotubes. In fact, Fig. 4 presents three peaks that appear at 330, 520 and 850 °C for 3WO_3/NT. The peaks that appear at 520 and 850°C are attributed to the reduction of

W^{6+} species [22]. The addition of rhodium nanoparticles (0.3 wt.%) to $3WO_3$/NT also modify its initial TPR profile. We found that appeared two new peaks at 117 and 155°C, which correspond to the reduction of Rh_2O_3 to metallic Rh^0. The further addition (from 0.3 to 0.5 wt.%) of Rh shifted the reduction peak from 117 to 155 C. The peak located between 270 and 470°C is ascribed to hydrogen consumed for the reduction of the strongly interacted RhO_x species formed at the interface between the metal (Rh) and the titanate nanotubes [23].

The increasing and decreasing reduction temperatures for rhodium and WO_3 on the titanate nanotubes, respectively, indicate the strong interaction between Rh and WO_3 species. According to the TPR results, the Rh species exist in their metallic state in the Rh-WO_3/NT photocatalysts. The Rh-WO_3 interaction may be attributed to either the electron transfer or oxygen transfer between the metal and reducible oxide [23].

3.5 Characterization by XPS

In order to observe the effect of rhodium on the $3WO_3$/NT photocatalysts, characterization by XPS was carried out for the 0.3Rh-$3WO_3$/NT and 0.5Rh-$3WO_3$/NT photocatalysts. Fig. 5(a) displays the W 4f core-level spectra that are characterized by two W $4f_{7/2}$ and W $4f_{5/2}$ peaks, which appear due to spin-orbital splitting [24]. The separation between the doublets is around 2.18 eV [24]. In addition, the 0.5Rh-$3WO_3$/NT photocatalyst showed the W $5p_{3/2}$ peak that is close to the W 4f core-level and is set at 5.5 eV above W $4f_{7/2}$ [24]. On the other hand, the characteristic binding energy of W $4f_{7/2}$ for the W^{5+} and W^{6+} species are located between 34–35 and 35–36 eV in the 0.3Rh-$3WO_3$/NT and 0.5Rh-$3WO_3$/NT photocatalysts.

With regard to 3d core-level spectra, it was difficult to carry out a correct deconvolution due to the low rhodium concentration. However, the presence the rhodium was confirmed on both 0.3Rh-$3WO_3$/NT and 0.5Rh-$3WO_3$/NT photocatalysts, as reported in Fig. 5(b). The 0.5Rh-$3WO_3$/NT

photocatalyst displays a low binding energy signal of $3d_{3/2}$ at 312 eV and Rh $3d_{5/2}$ at 307 eV, which may be related to the presence of Rh^{3+} species suggesting the formation of Rh_2O_3 [25]. In Fig 5(b) it is also observed a little shift to higher energies which led most species Rh_2O_3 in the 0.5Rh-$3WO_3$/NT photocatalyst than 0.3Rh-$3WO_3$/NT photocatalyst, suggesting that the increase from 0.3 to 0.5 wt.% of rhodium on $3WO_3$/NT photocatalysts allows more Rh oxide than Rh metal species. It is important to mention that due to the low content of Rh, we made a magnification. The results reported on Fig. 5(b) were multiplied by a factor of five to observe the Rh 3d spectrum, for this reason we do not carry out the deconvolution. Finally, the addition of 0.3 and 0.5 wt.% led to the splitting and appearance of W^{5+} species, but W^{6+} species prevailed mainly.

3.6. Photocatalytic activity

Fig. 6 presents the performance of the H_2 production activity at 365 nm on the NT, WO_3/NT, and Rh-WO_3/NT photocatalysts as a function of time for the run test (8 h). It is observed that 0.5Rh-$3WO_3$/NT photocatalyst showed a remarkable hydrogen production (234 µmol h^{-1}), which is almost 5 times higher than the hydrogen produced by photolysis (56 µmol h^{-1}), which is even 4 times more active than the $3WO_3$/NT (66 µmol h^{-1}) photocatalyst and 1.5 times higher than that of 0.5Rh-$3WO_3$/P25 (144 µmol h^{-1}). It is important to mention that rhodium (0.3 and 0.5 wt. %) and tungsten (3wt. %) loads are very low, however, they displayed notable photo-activity in the H_2 production. Table 2 presents the base-line production of hydrogen by the photolysis and photocatalysis processes. The photolysis of water produces 3 µmol h^{-1} of H_2. The photolysis of the water-2-propanol solution produces 56 µmol h^{-1}. The photocatalysis of water in the presence of 0.5Rh-$3WO_3$/NT photocatalyst produces 13 µmol h^{-1} of hydrogen. However, the addition of 2-propanol increases the hydrogen production up to 234 µmol h^{-1} on 0.5Rh-$3WO_3$/NT.

The results about stability are reported in Fig 7. The stability test was carried out using the 0.5Rh-$3WO_3$/NT photocatalyst, which showed the best H_2 production performance (234 μmol h^{-1}) during the first test. In the next five cycles (8 hours each one), 0.5Rh-$3WO_3$/NT photocatalyst showed an enhanced H_2 production with respect to the first cycle. 306 μmol h^{-1} of hydrogen was produced during the third cycle. Besides, the 0.5Rh-$3WO_3$/NT photocatalyst did not display any deactivation until the seventh cycle, where only 195 μmol h^{-1} were produced, which are equivalent to two days of continuous hydrogen production using the initial water–2-propanol solution. After two days of evaluation, we found that 0.5Rh-$3WO_3$/NT photocatalyst does not show deactivation.

It has been reported that [26], in presence of UV-365 nm illumination, the valence band electrons from TiO_2 nanotubular structure are excited to the conduction band, then they are transferred to the Rh nanoparticles and catalyze H^+/H_2 reactions for H_2 production [26]. Furthermore, the valence band electrons of WO_3 are excited to the conduction band and lead facilitate the oxidation of alcohol and then transferred to the valence band of TiO_2 nanotubular structure [26]. In our case, we suggest that Rh provide electrons and WO_3 provide holes to improve notably the hydrogen production from 66 μmol h^{-1} produced by $3WO_3$/NT to 234 μmol h^{-1} produced by 0.5Rh-$3WO_3$/NT photocatalyst. Likewise, 0.5Rh-$3WO_3$/NT photocatalyst shows very good stability and the H_2-evolution rates even after 56 h testing.

The H_2 production under visible light (at 450 nm) was also investigated. Fig. 8 shows the photocatalytic performance for the NT, $3WO_3$/NT and 0.5Rh-$3WO_3$/NT photocatalysts. As for the NT support, the H_2 production was not detected. The $3WO_3$/NT photocatalyst showed a small quantity of 13 μmol h^{-1} of hydrogen, which is in contrast with the addition of rhodium (0.5 wt. %) that exhibited the ability to produce H_2 under visible light, reaching a H_2 production of 87 μmol h^{-1} after eight hours. The results reported in the present work were compared with other photocatalytic systems and it was found that by using 1,000 mg of MWNT/TiO_2/Ni and methanol

as scavenger, 0.038 μmol h^{-1} were produced [27], carbon nanodots/WO_3 produced 1,330 μmol h^{-1} under a xenon lamp irradiation [28], and by using 100 mg of CdS/Pt/TiO_2 and Na_2S+Na_2SO_3 as scavenger, 4.2 μmol h^{-1} were produced [29]. In the case of the 0.5Rh-3WO_3/NT photocatalyst, it is possible that tungsten can be excited under visible light, leading to the generation and charge separation of electron-hole pairs transferred to the NT support in the conduction band and then transferred to rhodium.

On the other hand, the relationship between the semiconductor band structure and redox potentials for water splitting of the WO_3 conduction band should be lower than that of TiO_2. The bottom of the conduction band of WO_3 is lower than the H_2O/H_2 potential; likewise, WO_3 cannot be a photocatalyst for H_2 production. However, in this study, rhodium was identified as an attractive co-catalyst when added to WO_3/NT. In fact, the nanoparticles of Rh exert a remarkable positive effect on the H_2 production, since WO_3/NT is not active for H_2 production due to the low conduction band level under UV-365 and visible light (450 nm) irradiations. However, the combination of WO_3 and TiO_2 increases the UV photocatalytic activity due to the corresponding valence and conduction band energy levels favor not only the electron injection from the conduction band of TiO_2 to that of WO_3, but also the hole transfer between the valence bands in the opposite direction, which can reduce the electron–hole recombination in both semiconductors [30]. In fact, the addition of tungsten (3 wt.%) to the nanotubes gives as a result an outstanding resistance to deactivation for eight cycles.

Fig. 9 displays the production of hydrogen on 0.5Rh/NT photocatalyst for three cycles. This photocatalyst did not show deactivation after three cycles of eight hours. WO_3 is an element which is not suitable to produce hydrogen by itself. However, one characteristic of WO_3 is its remarkable photo-stability in aqueous solutions [31]. Furthermore, the combination Rh-WO_3 on titanate nanotubes enhances the hydrogen production and gives more stability during more cycles than

0.5Rh/NT photocatalyst. We can then conclude that WO_3 supported on titanate nanotubes acts as stabilizer and prevents the phase transformation (from $H_2Ti_3O_7$ to anatase phase) of the nanotubes during cycles. Furthermore, the ternary interaction (0.5 wt.%)Rh-(3 wt.%)WO_3-$H_2Ti_3O_7$ (0.5Rh-3WO_3/NT) promotes the hydrogen production from the water splitting process when compared to the corresponding hydrogen production from the 0.5Rh/NT and 3WO_3/NT photocatalysts.

3.7 Energy levels

The determination of the energy levels for the valence and conduction bands can be determined from the UV-vis results and from the XPS spectra, as reported by Ansari and Cho [32]. In this sense, and based in our results of XPS, we found that the valence band (VB) for NT is around 2.5 eV. The band gap energy (from the UV-vis spectrum reported in Table 1) for the NT is 3.33 eV. In consequence, the conduction band (CB) would occur at -0.8 eV. Following the procedure proposed for Ansari and Cho [32], we report the CB and VB structure for the NT, 3WO_3/NT and 0.5Rh-3WO_3/NT in Fig. 10.

We found that the VB for 3WO_3/NT is located at 2.1 eV, whereas the valence band maximum energy for 0.5Rh-3WO_3/NT was estimated at 1.7 eV, followed by a band tail around 0.4 eV. The band gap energy for 3WO_3/NT and 0.5Rh-3WO_3/NT are 2.75 and 3.55 eV, respectively. Therefore, the CB minimum for 3WO_3/NT and 0.5Rh-3WO_3/NT would occur at -0.6 and -1.8 eV, respectively. In this sense, the absorption onset in 3WO_3/NT and 0.5Rh-3WO_3/NT was located at 2.1 eV and 1.7 eV with a maximum energy associated with the band tail at 0.4 eV, respectively. We found that the presence of WO_3 and Rh in the titanate nanotubes simultaneously shifts the valence band maxima and conduction band minima, which help reduce the band gap of the titanate nanotubes. The observed narrowing of the band gap for 3WO_3/NT and 0.5Rh-3WO_3/NT respect to

that presented by NT may be due to the displacement and/or substitution of tungsten and Rh in the $H_2T_i3O_7$ lattice [32].

To enhance the water splitting reaction, in this work, the titanate nanotubes were doped with WO_3 and rhodium. WO_3 has a band gap energy of 2.77 eV. The position of the conduction band of WO_3 is located below of the reduction potential of the pair H_2/H^+, which is of 0.0 V in the electrochemical scale [33], therefore this oxide is inactive to produce H_2 because the photo-excited electrons do not have the right potential required to reduce protons from hydrogen. Indeed, the bottom of the conduction band (CB) is too low with respect to the H^+/H_2 redox potential [33]. However, doping of the $H_2Ti_3O_7$ with tungsten and rhodium seems to increase the electric conductivity due to is a higher valence ion W^{6+}, therefore enhances the electron transfer from the TiO_2 to the Rh, which promotes the H_2O dissociation [34].

Conclusions

The incorporation of nanoparticles of rhodium into the WO_3/NT photocatalyst plays an important role in the photocatalytic activity. We found that 0.5Rh-WO_3/NT enhanced the H_2 production 4 times more respect to the WO_3/NT photocatalyst. During the H_2 production from water-2-propanol, it was found that rhodium nanoparticles act as co-catalysts of the tungsten. However, WO_3 enhances the stability of the H_2 production on 0.5Rh-3WO_3/NT, which was active for six cycles of 8 hours, overmatching the first cycle.

These results indicated that the addition of Rh nanoparticles to WO_3/NT exerts a positive synergetic effect on the photocatalytic activity for the H_2 production of Rh-WO_3/NT with lamps of 365 and 450 nm. The combined effect of Rh and WO_3 nanoparticles resulted in a remarkable boosted H_2

production with respect to the WO_3/NT and NT photocatalysts, leading to an enhanced light absorption and increased charge separation.

Acknowledgments

We acknowledge the financial support provided by the Mexican Petroleum Institute through the Project D.00477, CONACyT and LINAN-IPICyT. Maria Isabel acknowledges support from the CIIEMAD-IPN to obtain the Master of Science Degree. IMC wishes to thank the hospitality of Dr. Luz. A. Serrano from CIIEMAD-IPN.

References

[1] Z. Wang and X. W. Lou, Adv. Mater. 24, (2012), 4124-4129.

[2] D. Chen and J. Ye, Adv. Funct. Mater. 18, (2008), 1922-1928.

[3] Q. Mi, A. Zhanaidarova, B. S. Brunschwig, H. B. Gray and N. S. Lewis, Energy Environ. Sci. 5, (2012), 5694-5700.

[4] D. D. Vuong, D. T. N. Tram, P. Q. Pho, N. D. Chien, D. T. Cat, A. Pucci and K. Wandelt, Springer, Berlin Heidelberg, 127, (2009), 95.

[5] V. Luca, M. G. Blackford, K. S. Finnie, P. J. Evans, M. James, M. J. Lindsay, M.S. Kazacos, P. R. F. Barnes, J. Phys. Chem. C 111, (2007), 18479-18492.

[6] J. Cai, X. Wu, S. Li, and F. Zheng, ACS Sustainable Chem. Eng. 4(3) (2016) 1581–1590.

[7] E.I. Yang, J-j. Shi, H-c. Liang, W-k. Cheuk, Chem. Eng. J. 174, (2011), 539–545.

[8] Y. Yamin, N. Keller, V. Keller, J. Photochem. Photobiol. A: Chem. 245, (2012), 43–57.

[9] Y.R. Smith, B. Sarma, S.K. Mohanty, M. Misra, Electrochem. Commun. 19, (2012), 131–134.

[10] P. Gomathisankar, D. Yamamoto, H. Katsumata, T. Suzuki, S. Kaneco, Int. J. Hydrog. Energy. 38, (2013), 5517–5524.

[11] H. Tian, S.Z. Kang, X. Li, L. Qin, M. Ji, J. Mu, Sol. Energy Mat. Sol. Cells. 134, (2015), 309–317.

[12] M.S. Park, M. Kang, Mater. Lett. 62, (2008), 183–187.

[13] H. Tian, X.L. Zhang, J. Scott, C. Ng, R. Amal, J. Mater. Chem. A. 2, (2014), 6432–6438.

[14] K. Maeda, K. Teramura, K. Domen, Catal Surv Asia. 11, (2007), 145-157.

[15] Y. Yuan, J. Lv, X. Jiang, Z. Li, T. Yu, Z. Zou, J. Ye, Appl. Phys. Lett. 91, (2007), 094107.

[16] D. Jing L. Guo, J. Phys. Chem. B. 110, (2006), 11139-11145.

[17] R. Camposeco, S. Castillo, Isidro Mejía-Centeno, J. Navarrete, N. Nava, V. Rodríguez-González, J. Photochem. Photobiol. A: Chem. 341 (2017) 87–96

[18] Q. Chen, G.H. Du, S. Zhang, L. Peng, Acta Cryst. B58, (2002), 587-593

[19] S.J. Gregg, K.S.W. Sing, Adsorption, Surface Area and Porosity, second ed., Academic Press, London, (1974).

[20] V. Iliev, D. Tomova, S. Rakovsky, A. Eliyas, and G. Li Puma, J. Mol. Catal. A: Chemical. 327, (2010), 51–57.

[21] Weller, H., Eychmüller, A. Semiconductor Nanoclusters; Elsevier Science; Amsterdam, 1996.

[22] M.A. Reiche, M. Maciejewski, A. Baiker, Catal. Today. 56, (2000), 347–355.

[23] J.C. Vis, H.F.J. Van't Buk , T. Huizinga, T. Huizinga, R. Prins. Journal of Molecular Catalysis A: Chemical. 25, (1984), 367 378.

[24] I. Kojima and M. J. Kurahashi, J. Electron Spectrosc. Relat. Phenom. 42, (1987), 177–181.

[25] S. Suhonen, M. Valden, M. Hietikko, R. Laitinen, A. Savimaki and M. Harkonen, Appl. Catal., A, 218, (2001), 151-160.

[26] H. Gao, P. Zhang, J. Hu, J. Pan, J. Fan, G. Shao, Applied Surface Science. 391, (2017), 211-217.

[27] Y. Ou, J. Lin, S. Fang, D. Liao, Chem. Phys. Lett. 429, (2006), 199–203.

[28] L. Qi, J. Yu, M. Jaroniec, Phys. Chem. Chem. Phys. 13, (2011), 8915–8923.

[29] P. Yang, J. Zhao, J. Wang, B. Cao, L. Lia and Z. Zhu, J. Mater. Chem. A, 3, (2015), 8256-8259.

[30] J. Georgieva, .Valova, S. Armyanov, N. Philippidis, I. Poulios, S. Sotiropoulos, J. Hazard Mater. 211-222, (2012), 30–46.

[31] D. Monllor-Satoca, L. Borja, A. Rodes, R. Gómez and P. Salvador. Chem. Phys. Chem., 7, (2006), 2540-2551.

[32] S. A. Ansari and M. H. Cho, Sci. Rep, 6, (2016), 25405.

[33] P. Li, G. Zhao, X. Cui, Y. Zhang, Y. Tang, J. Phys. Chem. C, 113, (2009) 2375–2383.

[34] . F. Wang, C. D. Valentin, G. Pacchioni, Chem. Cat. Chem., 4, (2012) 476–4788.

Figure captions

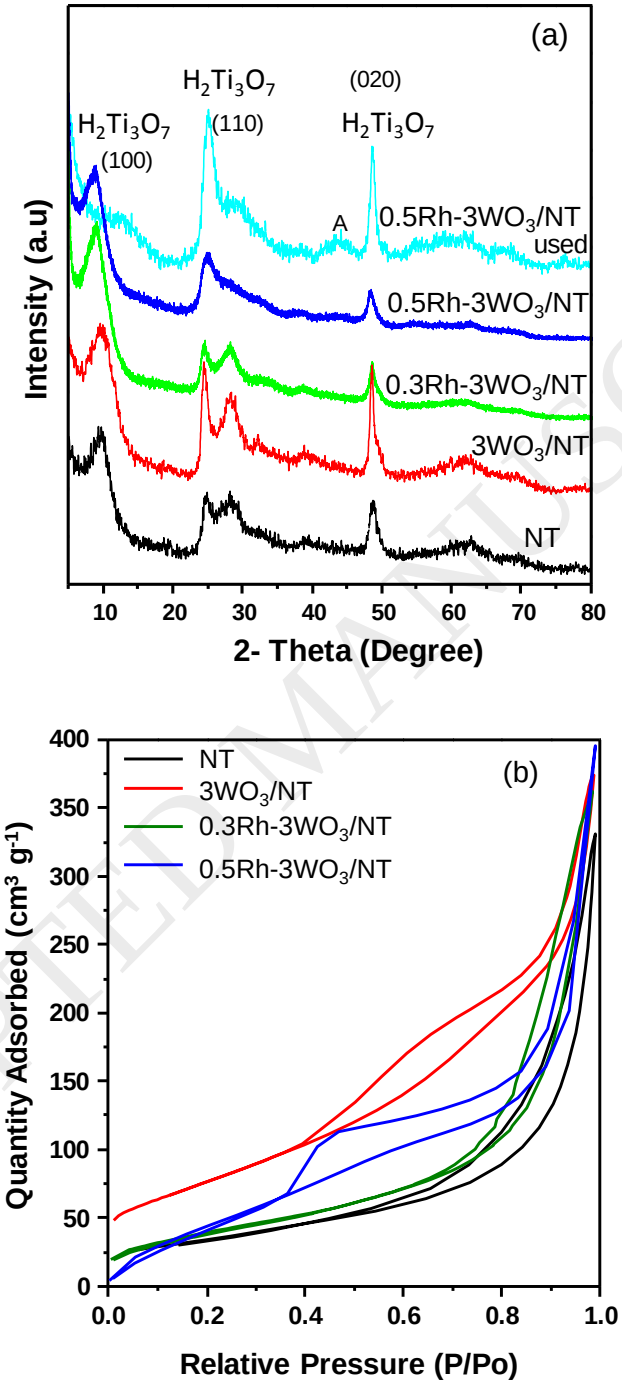

Fig. 1. (a) XRD patterns for WO_3/NT, Rh-WO_3/NT photocatalysts annealed at 300°C. $H_2Ti_3O_7$ is the trititanic acid phase and **(b)** N_2 adsorption-desorption isotherms for NT, WO_3/NT and Rh-WO_3/NT catalysts. A means anatase phase.

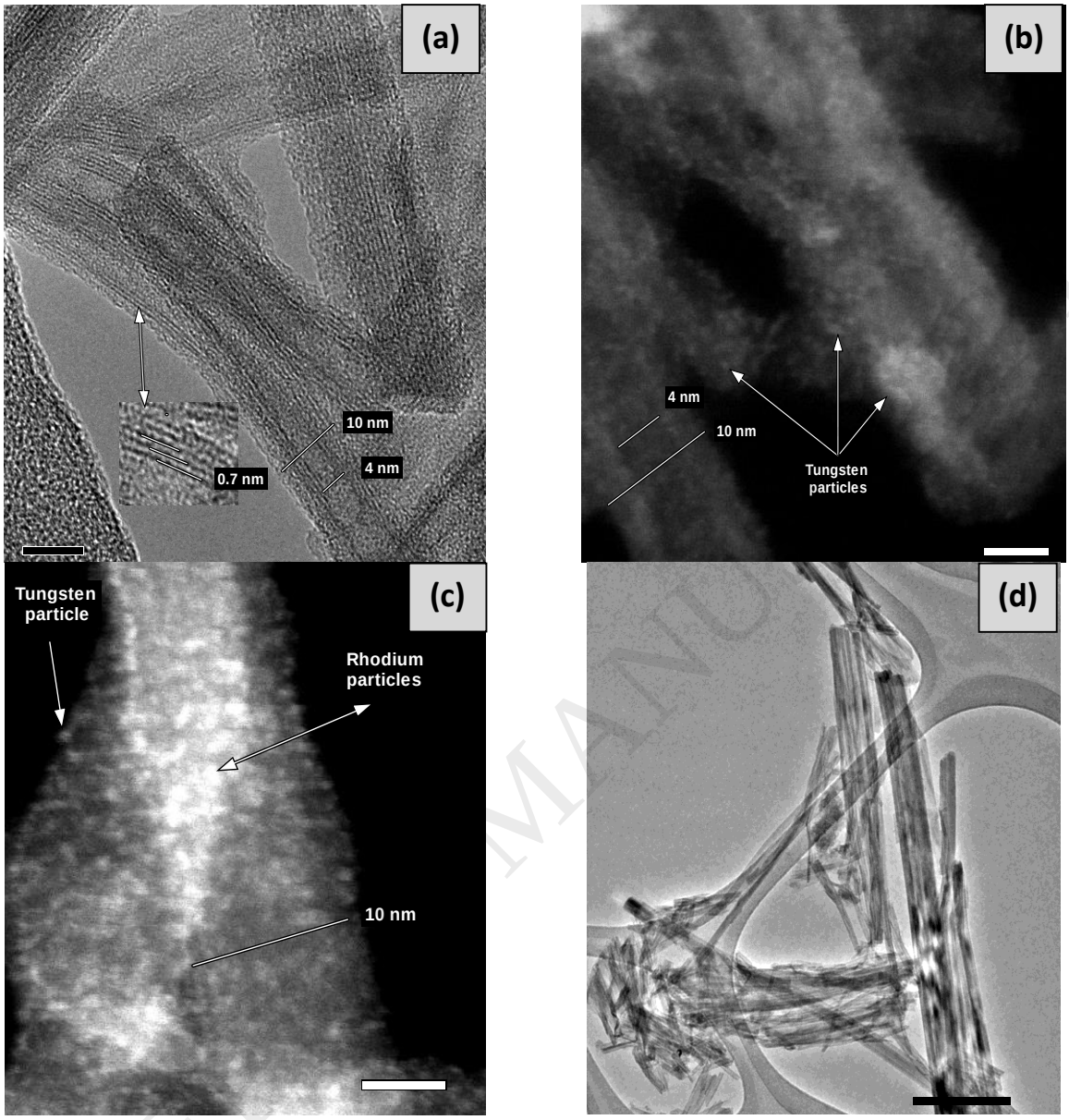

Fig. 2. HR-TEM for (a) NT, (b) $3WO_3$/NT, (c) 0.5Rh-$3WO_3$/NT annealed at 300°C, (d) HR-TEM for spent 0.5Rh-$3WO_3$/NT photocatalyst.

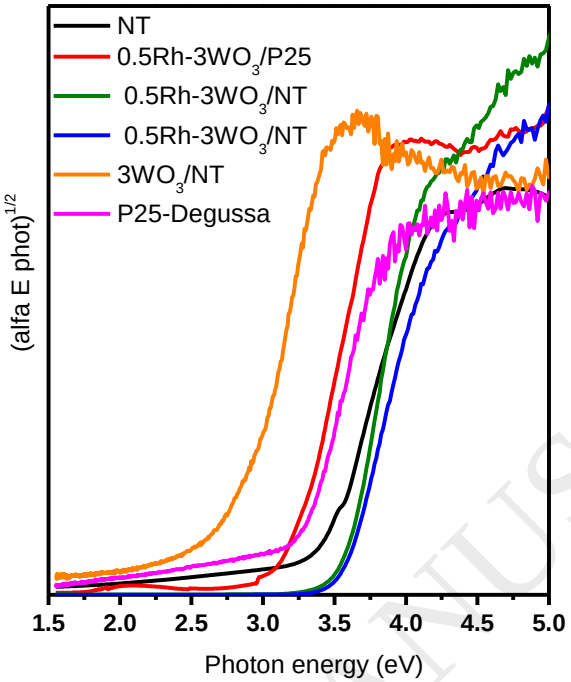

Fig. 3. UV-vis spectra for NT, $3WO_3$/NT, 0.3Rh-$3WO_3$/NT and 0.5Rh-$3WO_3$/NT photocatalysts annealed at 300°C.

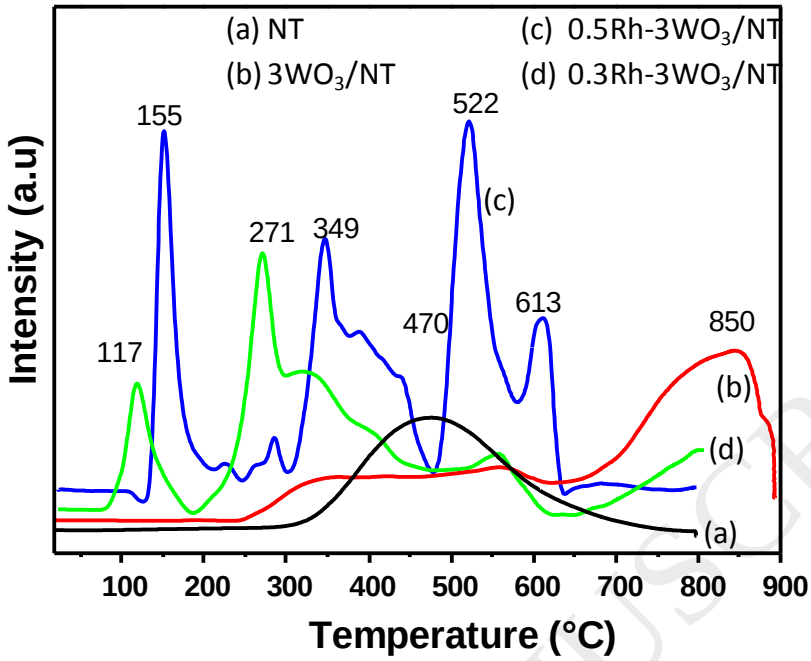

Fig. 4. H_2-TPR profiles for NT, $3WO_3$/NT, 0.3Rh-$3WO_3$/NT and 0.5Rh-$3WO_3$/NT photocatalysts

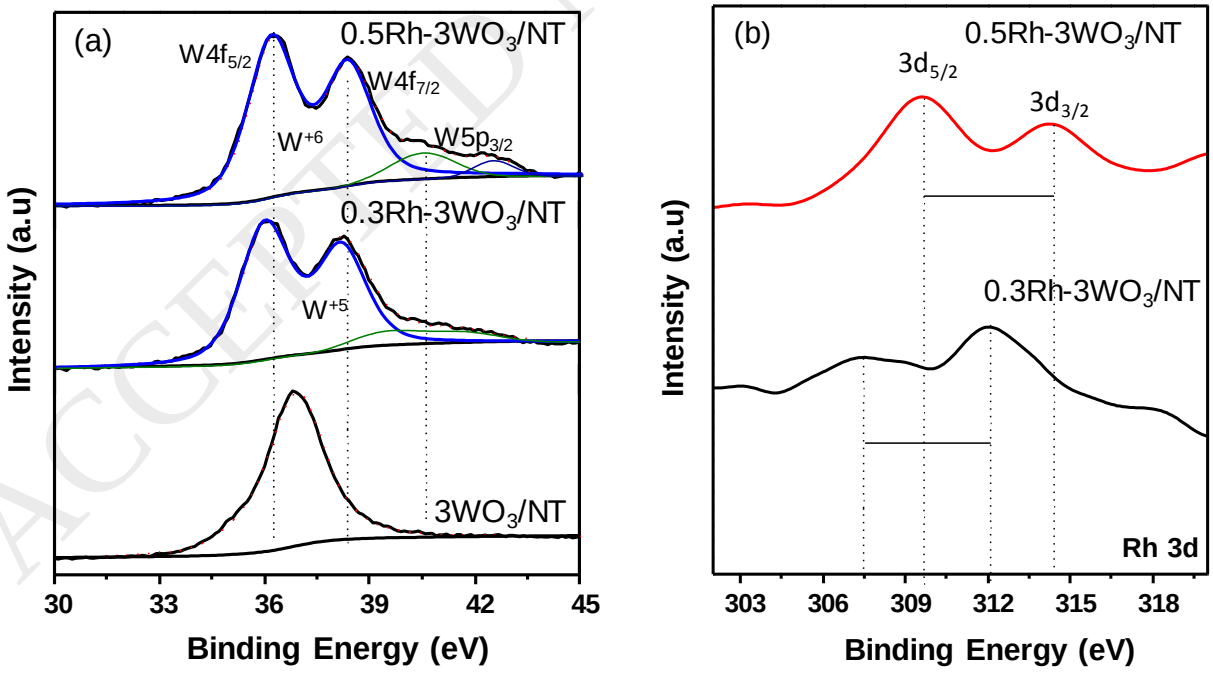

Fig. 5. (a) XPS high-resolution spectra over W4f peaks for $3WO_3$/NT and 0.5Rh-$3WO_3$/NT photocatalysts and **(b)** XPS spectra over Rh3d peaks for Rh-WO_3/TiO_2 photocatalysts. The Rh 3d spectra were multiplied by five.

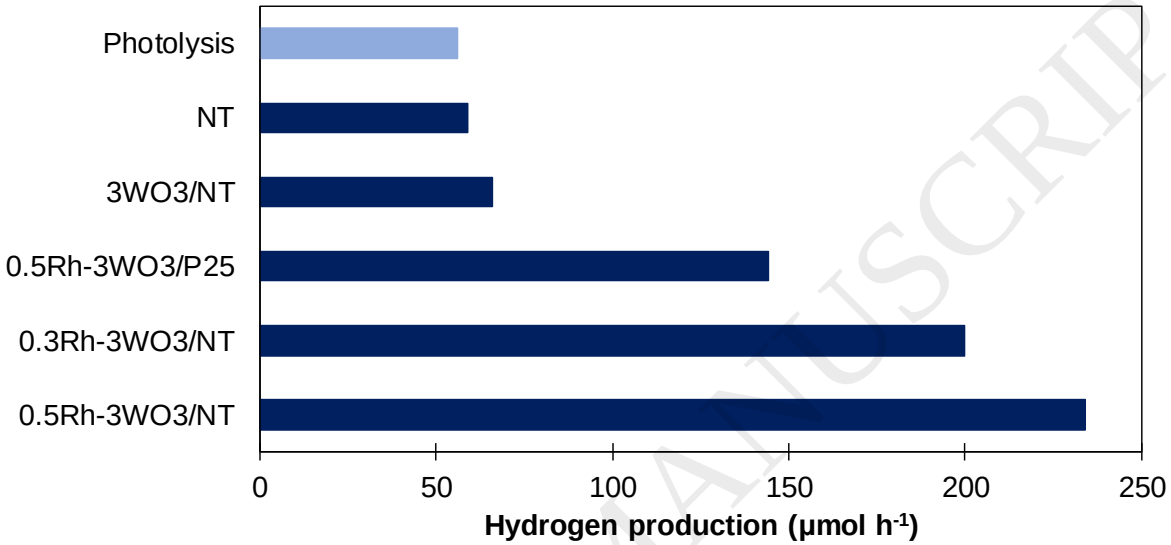

Fig. 6. H_2 production for NT, $3WO_3$/NT, 0.3Rh-$3WO_3$/NT and 0.5Rh-$3WO_3$/NT photocatalysts with 0.05g of photocatalysts using water–2-propanol solution

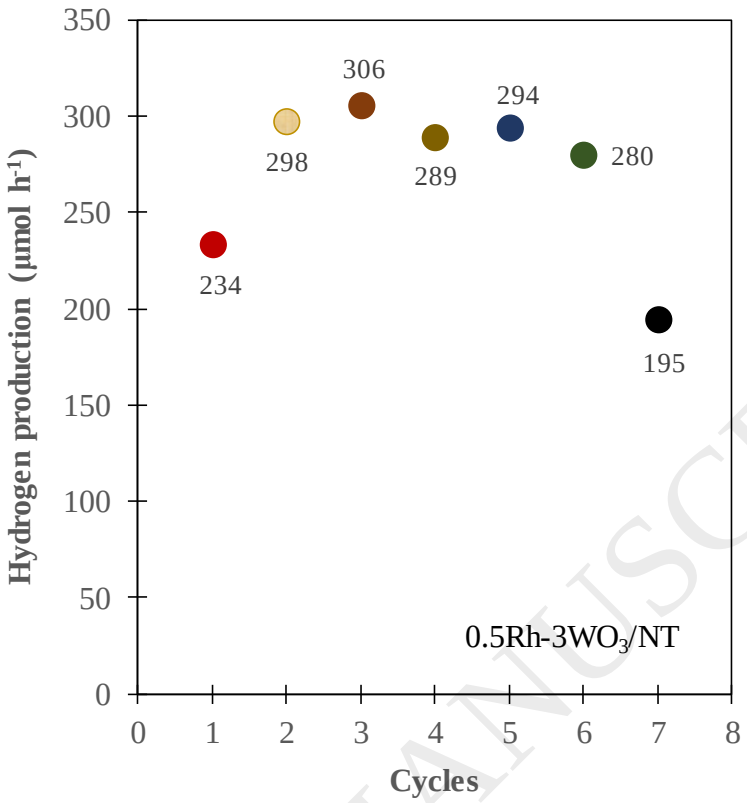

Fig. 7. H_2 production for 0.5Rh-3WO_3/NT photocatalyst for seven cycles. 8 h per cycle

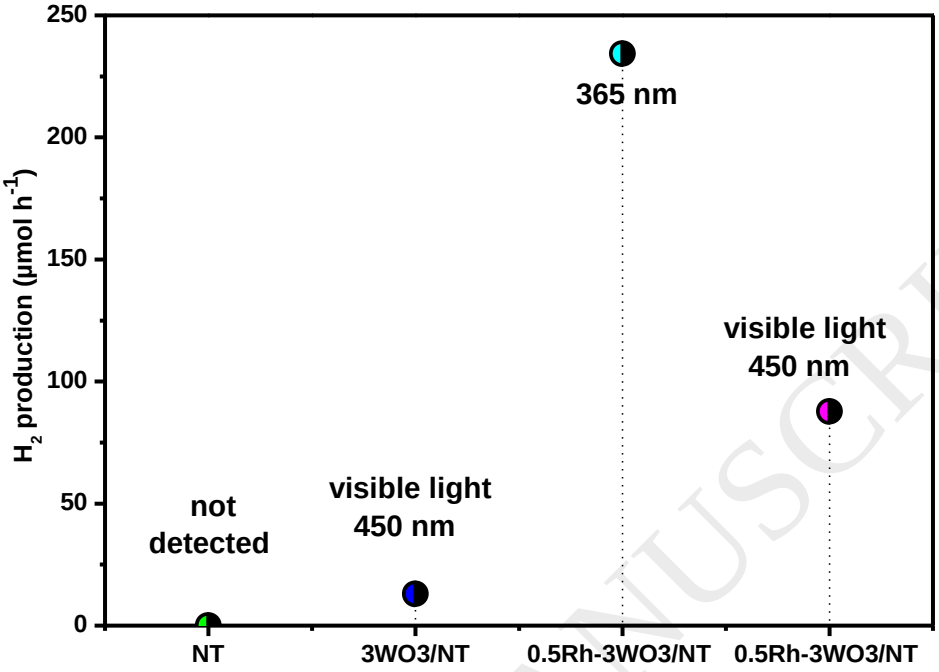

Fig. 8. H_2 production for NT and 0.5Rh-3WO_3/NT using visible light of 450 nm

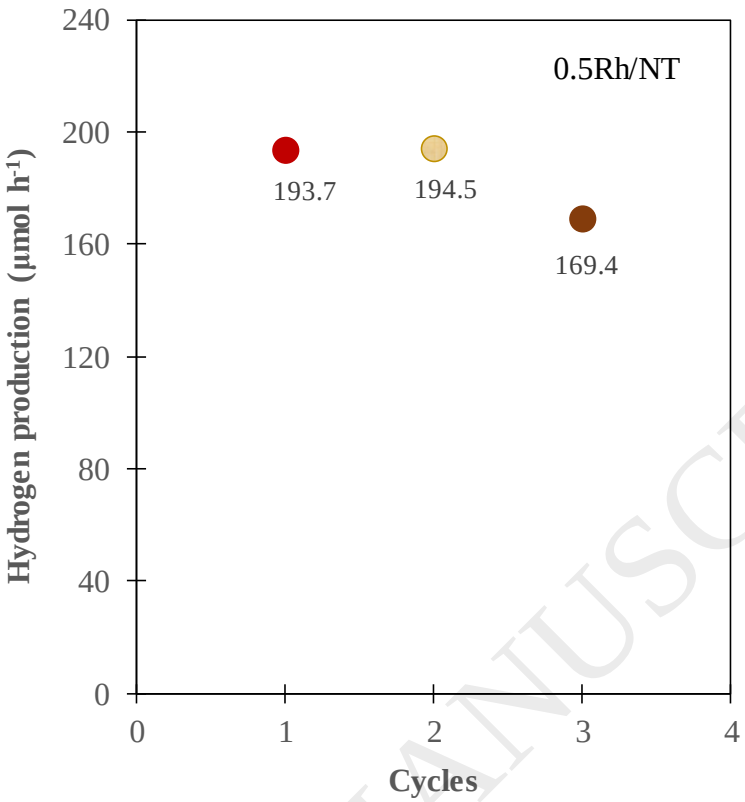

Fig. 9. H_2 production on 0.5Rh/NT photocatalyst for three cycles.

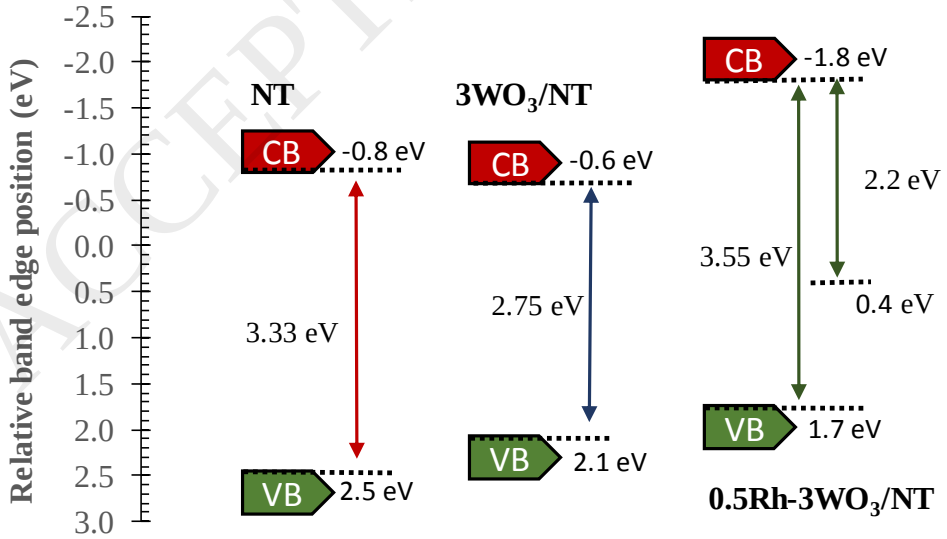

Fig. 10. Schematic diagram of the density of states for NT, $3WO_3$/NT and 0.5Rh-$3WO_3$/NT.

Table 1.

Physicochemical properties of WO_3/NT, Rh-WO_3/NT photocatalysts annealed at 300°C.

Sample	S_{BET} (m^2/g)	Phase	Band Gap (eV)
NT	282	$H_2Ti_3O_7$	3.33
3WO_3/NT	323	$H_2Ti_3O_7$	2.75
0.3Rh-3WO_3/NT	299	$H_2Ti_3O_7$	3.45
0.5Rh-3WO_3/NT	302	$H_2Ti_3O_7$	3.55
0.5Rh-3WO_3/P25	55	Anatase/Rutile	3.10
P-25-Degussa	52	Anatase/Rutile	3.24

Table 2.

Hydrogen production by photocatalyst and photolysis under UV radiation at 365 nm

Sample	H_2 production (μmol h^{-1})	H_2 production (μmol $h^{-1}.g^{-1}$)
NT	59	1180
3WO_3/NT	66	1320
0.3Rh-3WO_3/NT	200	4000
0.5Rh-3WO_3/NT	234	4680
0.5Rh-3WO_3/P25	144	2880
0.5Rh-3WO_3/NT (Water)	13	260
Photolysis (Water)	3	
Photolysis (Water-2-propanol)	56	